# Thermal-Mechanical Stability of Single Crystal Oxide Refractive Concentrators for High-Temperature Solar Thermal Propulsion

Dongming Zhu, Nathan S. Jacobson, and Robert A. Miller
Lewis Research Center, Cleveland, Ohio

Since its founding, NASA has been dedicated to the advancement of aeronautics and space science. The NASA Scientific and Technical Information (STI) Program Office plays a key part in helping NASA maintain this important role.

The NASA STI Program Office is operated by Langley Research Center, the Lead Center for NASA's scientific and technical information. The NASA STI Program Office provides access to the NASA STI Database, the largest collection of aeronautical and space science STI in the world. The Program Office is also NASA's institutional mechanism for disseminating the results of its research and development activities. These results are published by NASA in the NASA STI Report Series, which includes the following report types:

- TECHNICAL PUBLICATION. Reports of completed research or a major significant phase of research that present the results of NASA programs and include extensive data or theoretical analysis. Includes compilations of significant scientific and technical data and information deemed to be of continuing reference value. NASA's counterpart of peer-reviewed formal professional papers but has less stringent limitations on manuscript length and extent of graphic presentations.

- TECHNICAL MEMORANDUM. Scientific and technical findings that are preliminary or of specialized interest, e.g., quick release reports, working papers, and bibliographies that contain minimal annotation. Does not contain extensive analysis.

- CONTRACTOR REPORT. Scientific and technical findings by NASA-sponsored contractors and grantees.

- CONFERENCE PUBLICATION. Collected papers from scientific and technical conferences, symposia, seminars, or other meetings sponsored or cosponsored by NASA.

- SPECIAL PUBLICATION. Scientific, technical, or historical information from NASA programs, projects, and missions, often concerned with subjects having substantial public interest.

- TECHNICAL TRANSLATION. English-language translations of foreign scientific and technical material pertinent to NASA's mission.

Specialized services that complement the STI Program Office's diverse offerings include creating custom thesauri, building customized data bases, organizing and publishing research results . . . even providing videos.

For more information about the NASA STI Program Office, see the following:

- Access the NASA STI Program Home Page at *http://www.sti.nasa.gov*

- E-mail your question via the Internet to help@sti.nasa.gov

- Fax your question to the NASA Access Help Desk at (301) 621-0134

- Telephone the NASA Access Help Desk at (301) 621-0390

- Write to:
  NASA Access Help Desk
  NASA Center for AeroSpace Information
  7121 Standard Drive
  Hanover, MD 21076

# Thermal-Mechanical Stability of Single Crystal Oxide Refractive Concentrators for High-Temperature Solar Thermal Propulsion

Dongming Zhu, Nathan S. Jacobson, and Robert A. Miller
Lewis Research Center, Cleveland, Ohio

National Aeronautics and
Space Administration

Lewis Research Center

# Acknowledgments

Available from

# Thermal-Mechanical Stability of Single Crystal Oxide Refractive Concentrators for High-Temperature Solar Thermal Propulsion

Dongming Zhu
Ohio Aerospace Institute
Brook Park, OH 44142
E-mail:Dongming.Zhu@lerc.nasa.gov

Nathan S. Jacobson and Robert A. Miller
NASA Lewis Research Center
21000 Brookpark Road
Cleveland, OH 44135

## ABSTRACT

Single crystal oxides such as yttria-stabilized zirconia ($Y_2O_3$-$ZrO_2$), yttrium aluminum garnet ($Y_3Al_5O_{12}$, or YAG), magnesium oxide (MgO) and sapphire ($Al_2O_3$) are candidate refractive secondary concentrator materials for high temperature solar propulsion applications. However, thermo-mechanical reliability of these components in severe thermal environments during the space mission sun/shade transition is of great concern. Simulated mission tests are important for evaluating these candidate oxide materials under a variety of transient and steady-state heat flux conditions, and thus provide vital information for the component design. In this paper, a controlled heat flux thermal shock test approach is established for the single crystal oxide materials using a 3.0 kW continuous wave $CO_2$ laser, with a wavelength 10.6 micron. Thermal fracture behavior and failure mechanisms of these oxide materials are investigated and critical temperature gradients are determined under various temperature and heating conditions. The test results show that single crystal sapphire is able to sustain the highest temperature gradient and heating-cooling rate, and thus exhibit the best thermal shock resistance, as compared to the yttria-stabilized zirconia, yttrium aluminum garnet and magnesium oxide.

## INTRODUCTION

Recently refractive secondary solar concentrator systems have been developed for solar thermal power and propulsion applications [1]. A well-designed refractive

secondary concentrator system possesses higher solar concentration ratio and efficiency, and better flux tailoring within the heat receiver cavity, as compared to the conventional hollow reflective parabolic concentrator systems [1, 2]. Single crystal oxides such as yttria-stabilized zirconia ($Y_2O_3$-$ZrO_2$), yttrium aluminum garnet ($Y_3Al_5O_{12}$, or YAG), magnesium oxide (MgO) and sapphire ($Al_2O_3$) are candidate refractive secondary concentrator materials. However, the refractive concentrator system will experience high temperature and thermal cycling in the solar thermal engine during the space mission sun/shade transition and therefore thermal mechanical reliability of the oxide components in the severe thermal environments is of great concern. Finite element analysis shows that for a cubic $ZrO_2$-$Y_2O_3$ single crystal concentrator system, a peak temperature of 1800°C at the tip of the concentrator flux extractor and a temperature difference up to 1500°C across the 25.4 mm region of the concentrator-extractor interface may be established during the heat-up cycles [3].

The purpose of this paper is to establish appropriate test techniques to evaluate the thermo-mechanical stability of four different candidate single crystal oxide materials, under space mission thermal gradient and heat flux conditions. Thermal stress resistance, thermal fracture behavior and failure mechanisms of these single crystal are investigated under steady-state and transient heat flux conditions. Critical temperature gradients and corresponding absorbed power densities imposed on the crystals to cause failure, are determined for various temperature and heating conditions that these materials are expected to experience in refractive concentrator applications.

## EXPERIMENTAL MATERIALS AND METHODS

### Materials

Single crystal oxides including 20%$Y_2O_3$-doped cubic zirconia ($Y_2O_3$-$ZrO_2$), yttrium aluminum garnet ($Y_3Al_5O_{12}$ or YAG), magnesium oxide (MgO) and sapphire ($Al_2O_3$) were obtained from a commercial source (ONYX Optics, Inc., 6551 Sierra lane, Dublin, California). The materials were machined into 25.4 mm diameter circular disk specimens (thickness 1 mm), and 12.7 mm diameter cylindrical specimens (length 12.7

mm or 25.4 mm). The surfaces of the disk and cylinder specimens were parallel to the major crystallographic planes of these crystals, namely, (100) plane for $ZrO_2$-$Y_2O_3$ and MgO, (111) plane for YAG, and (0001) plane for $Al_2O_3$ (sapphire). These surface plane directions of the specimens were thus consistent with the optical axes of the actual components. For the $ZrO_2$-$Y_2O_3$ and MgO materials, $12.7 \times 12.7 \times 12.7$ mm cube specimens with the (100) orientation surfaces were also used. The crystallographic orientations of the specimen surfaces were confirmed using X-ray Laue diffraction. Specimen surfaces were polished to a mirror finish on all sides before each test.

**Thermal Expansion and Room Temperature Hardness Tests**

Thermal expansion experiments were carried out on all the single crystals, in air, using a high temperature dilatometer system. The 25.4 mm-long cylindrical specimens were used for the thermal expansion measurements, and a platinum standard specimen was used as reference. Since yttria-doped $ZrO_2$, MgO and YAG have cubic structures, and it is normally assumed that these materials are isotropic, the material thermal expansions were measured only in their component optical axis directions ([100] direction for $ZrO_2$ and MgO, and [111] direction for YAG). For anisotropic sapphire, however, thermal expansions were measured not only in the optical axis direction [0001] using the 25.4 mm-long cylindrical specimen, but also in the directions perpendicular to its [0001] axis using the 25.4 mm diameter thin disk specimens.

Room-temperature Knoop hardness tests were conducted using a Knoop indenter on yttra-doped $ZrO_2$ (100), MgO (100), YAG (111) and $Al_2O_3$ (0001) surfaces, in accordance with ASTM C1326. The load used was 500 g and dwell time was 15 seconds. For each specimen, a total of twenty measurements were made, and average hardness values were obtained for the materials.

**The Steady-State Thermal Gradient Test and Transient Thermal Shock Test**

A 3.0 kW $CO_2$ continuous wave (wavelength 10.6 $\mu m$) laser was used to provide controlled surface heating for the oxide specimens. A schematic diagram of the laser test rig used for this high-temperature thermal gradient testing is illustrated in Figure 1. The

$CO_2$ laser is especially well-suited for the single crystal thermal shock tests because it can directly deliver well-characterized heat energy to the oxide surfaces. Since the oxides are opaque at the 10.6 $\mu m$ wavelength of laser beam, the light energy is absorbed at the surfaces rather than transmitting into the crystals, and thus generating the required temperature gradients within the specimens. In order to provide more uniform heating over the entire specimen surface, the relatively sharp raw beam with a diameter of 13 mm was expanded to a broader beam size with a diameter of 40 mm, using a ZnSe (focal length 63.5 mm) positive meniscus lens. The resulting laser beam profile was measured on a PC laser beam analyzer by capturing a thermal image of a 0.5-second laser pulse. The measured power density distribution of the expanded laser beam is shown in Figure 2. Despite of a 15% difference in the laser beam energy distribution between the peak and valley, a fairly uniform surface heating was observed by thermography even for the 25.4 mm diameter disk specimens.

Steady-state thermal gradient tests were conducted on the thin disk specimens to determine the critical temperature differences across the specimen thickness to initiate cracking. A temperature gradient was established through the specimen thickness by laser direct surface heating and backside air cooling. The laser power (thus the heat flux) was continuously increased at a slow rate, so a pseudo-steady-state heating of the specimen was always achieved and the temperature gradient across the specimen thickness increased with the heating time. Since the disk specimen immediately broke off once the crack was initiated, the onset of the cracking and fracture of the specimen was recorded as a sudden temperature drop in the pyrometer temperature reading. The specimen failure temperatures can be roughly controlled by adjusting the cooling. The critical temperature difference was thus determined for each specimen at various specimen back temperatures.

The thermal gradient testing of the single crystal cylindrical specimens was also carried out to simulate the heating/cooling cycles during the space mission. In this experiment, indirect laser heating (by laser-heated superalloy plate thermal conduction) was used to ensure extremely slow surface heating (Figure 1 (b)). Surface temperature

was measured by a type-R thermocouple at the back side of the laser heated superalloy heating plate near the specimen. Specimen cracking was monitored from a video camera and real-time thermography images. The specimens were inspected after each cycle.
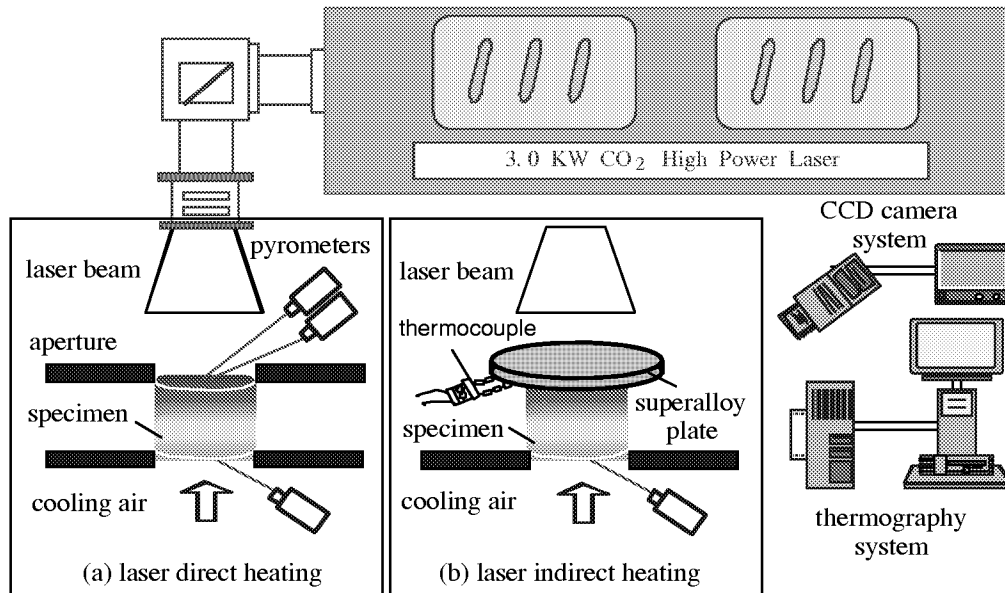


Fig.1 Schematic diagram showing high temperature thermal gradient testing of candidate refractive solar concentrator oxide materials using a high power laser. The laser power is measured using an internal power meter. The surface and back temperatures, and temperature distributions of the specimen are monitored by 8-$\mu m$ pyrometers, and a 3 $\mu m$ thermography unit. Thermocouples are also used in temperature measurements of laser indirect heating. All data are recorded in a computer system.

Laser transient thermal shock tests were conducted on the cylindrical single crystal specimens using a direct laser beam heating approach. Laser power was increased in approximately 30 W increments and the specimen was heated for a total time of 60 seconds. Specimen cracking was also monitored using a video camera and real-time thermography. The critical laser power density resulting in specimen fracture was thus determined for each specimen. For each material, two specimens were tested and an average critical power value was chosen. During the test, heating/cooling profiles and

temperature distributions were experimentally measured with thermography and pyrometry, and were also compared with the analytical solutions [4] and one-dimensional (one–D) finite difference models described previously [5, 6].

Microstructural evidence to help explain thermal fracture behavior and failure mechanisms of these oxide materials was examined after each test using optical and scanning electron microscopy.
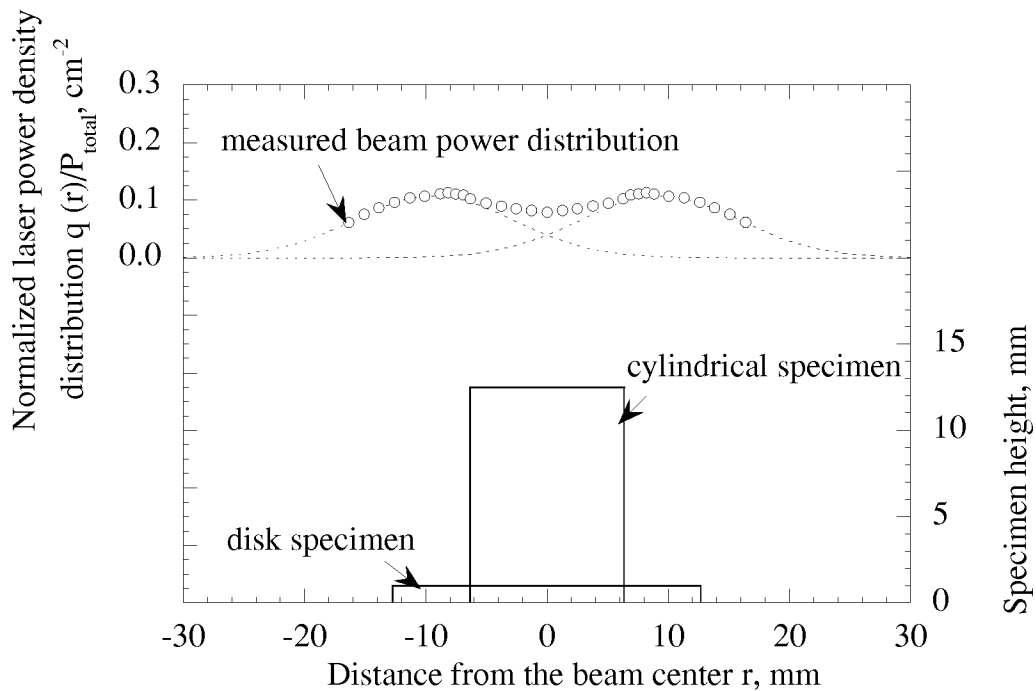


Fig. 2    The measured power density distribution $q(r)$ of the expended laser beam. Note that the power density distribution shown is normalized with respected to the total laser power $P$.

## EXPERIMENTAL RESULTS AND DISCUSSION

Figure 3 shows the thermal expansion behavior of the single crystal materials up to a temperature of 1400°C. It can be seen that MgO has the highest coefficient of thermal expansion (CTE), while sapphire has the lowest coefficient of thermal expansion (CTE).

The average CTE values for these materials are: $10.6 \times 10^{-6}$ m/m - °C for yttria-doped $ZrO_2$, $9.2 \times 10^{-6}$ m/m - °C for YAG, $13.8 \times 10^{-6}$ m/m - °C for MgO, $8.9 \times 10^{-6}$ m/m - °C for $Al_2O_3$ parallel to [0001] direction and $8.6 \times 10^{-6}$ m/m - °C for $Al_2O_3$ perpendicular to [0001], respectively.

Figure 4 shows the room-temperature hardness measurement results. Among these oxides, $Al_2O_3$ has the highest hardness, whereas MgO has the lowest hardness. Yttria-doped $ZrO_2$ and YAG have almost equivalent hardness values. The average Knoop hardness values are $11.25 \pm 0.39$ GPa for $Y_2O_3$-doped $ZrO_2$, $11.13 \pm 0.37$ GPa for YAG, $3.73 \pm 0.24$ GPa for MgO, $15.01 \pm 0.53$ GPa for $Al_2O_3$.
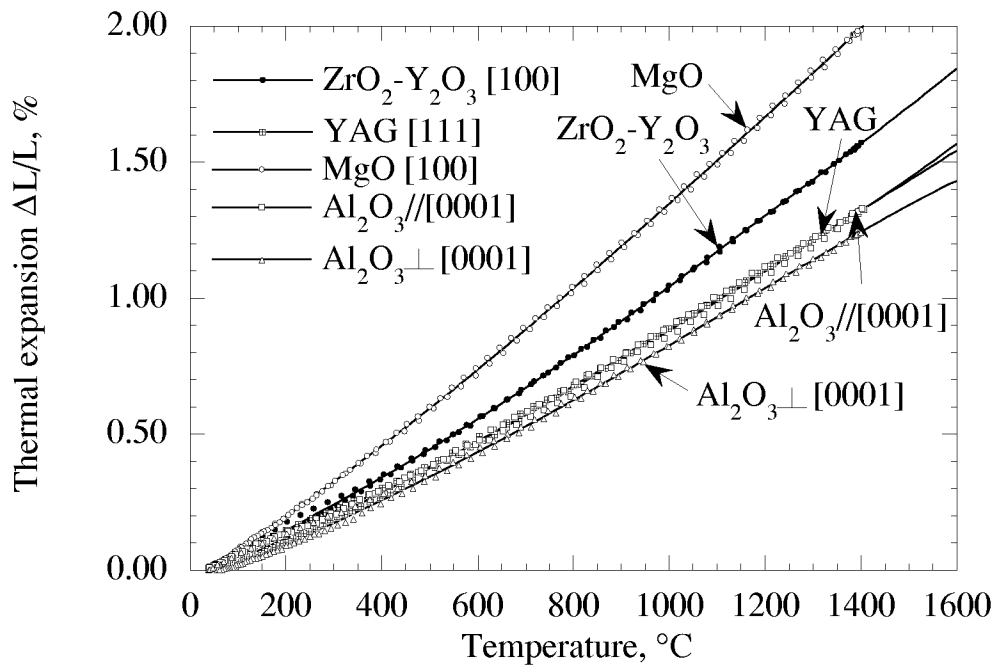


Fig. 3    Thermal expansion behavior of single crystal $Y_2O_3$-doped $ZrO_2$, YAG, MgO, and $Al_2O_3$ (sapphire) oxides.
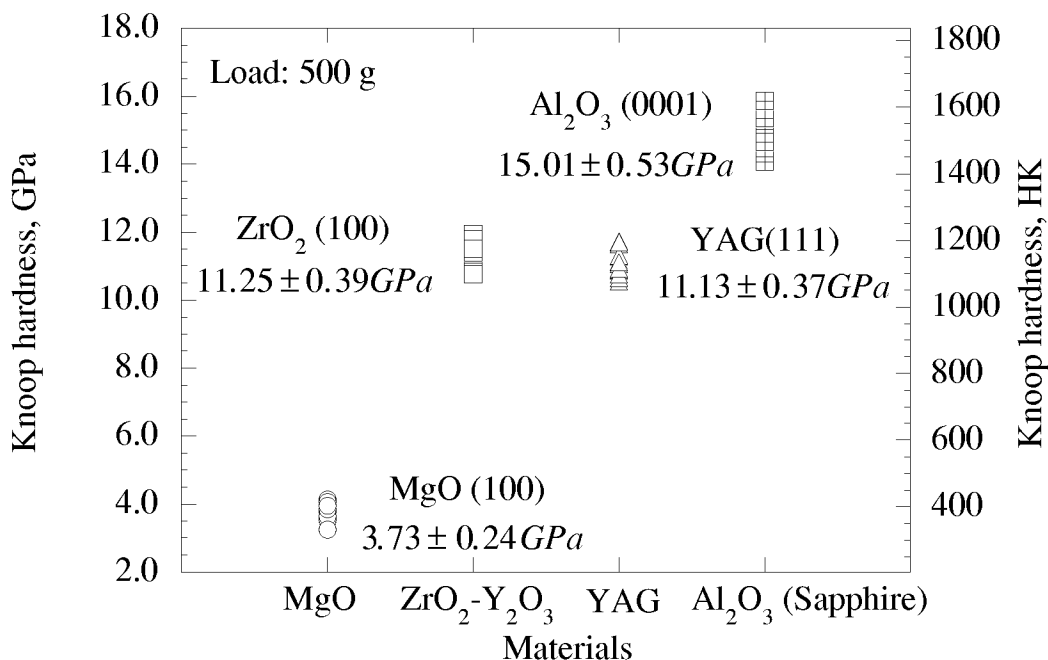
Fig. 4    Knoop hardness measurement results of single crystal $Y_2O_3$-doped $ZrO_2$, YAG, MgO, and $Al_2O_3$ (sapphire) oxides.

Figure 5 illustrates examples of the heating profiles of the $Y_2O_3$-doped $ZrO_2$, YAG, and $Al_2O_3$ (sapphire) disk specimens during the laser steady-state thermal gradient testing. The critical temperature difference and corresponding power density to cause failure were readily determined at the onset of specimen cracking. The test results for all the specimens are shown in Figure 6. The $Y_2O_3$-doped $ZrO_2$ and YAG oxides exhibited a similar thermal stress resistance, with the average critical temperature differences being $81 \pm 20°C$ and $88 \pm 21°C$, respectively. In contrast, the $Al_2O_3$ oxide showed a much better thermal stress resistance. The critical temperature difference for $Al_2O_3$ was $200 \pm 35°C$. The $Al_2O_3$ specimens also exhibited a higher thermal stress resistance at higher temperatures. The critical laser power densities at failure for $Y_2O_3$-doped $ZrO_2$, YAG and $Al_2O_3$ disk specimens were approximately 21 $W/cm^2$, 72 $W/cm^2$ and 177 $W/cm^2$, respectively. Note that the critical power density values are corresponding to the total

absorbed laser light energy in the crystals. Considering that thermal gradients established in the secondary solar concentrator systems are due to the heat receiver cavity heating/cooling cycles [3] and to a small portion of solar light energy absorbed in the crystal components, the information obtained from this experiment can be of great importance in component design.

Since the temperature gradient in the specimen resulting from the steady-state heating will impose a compressive stress state in the surface region of the disk specimen, tensile stress would usually be generated near the backside of the specimen. Crack initiation is thus likely to occur near the back surface for the thin specimen, because oxides are much weaker in tension than in compression. The fractographs from the scanning microscope confirmed this type of failure. Figure 7 illustrates the $Y_2O_3$-$ZrO_2$ case. Note that the crack origins were typically observed near the back edges of the specimen. The critical temperature difference, $\Delta T$, across the specimen under the steady state heating condition is closely related to the material strength [7, 8]. It is found that the Vickers or Knoop indentation hardness values for oxide systems are closely related to the oxide apparent atomic volumes of oxygen, and thus, to a certain extent, are reflecting the strength of the interatomic bonding [9]. Therefore, the critical $\Delta T$ at the low temperature regime (e.g., below 600°C), is believed to be roughly associated with the measured room-temperature Knoop hardness values. Sapphire ($Al_2O_3$), which has the highest hardness value, showed the best thermal stress resistance. The increased $\Delta T$ for $Al_2O_3$ specimens at higher temperatures may be related to possible microscale stress relaxation due to the inelastic deformation and the reduced modulus value. Surface polish as well as edge-preparation conditions can also dramatically affect these properties. The complicate effects of the test temperature and specimen preparation conditions may explain the relatively large data scatter observed in this study.
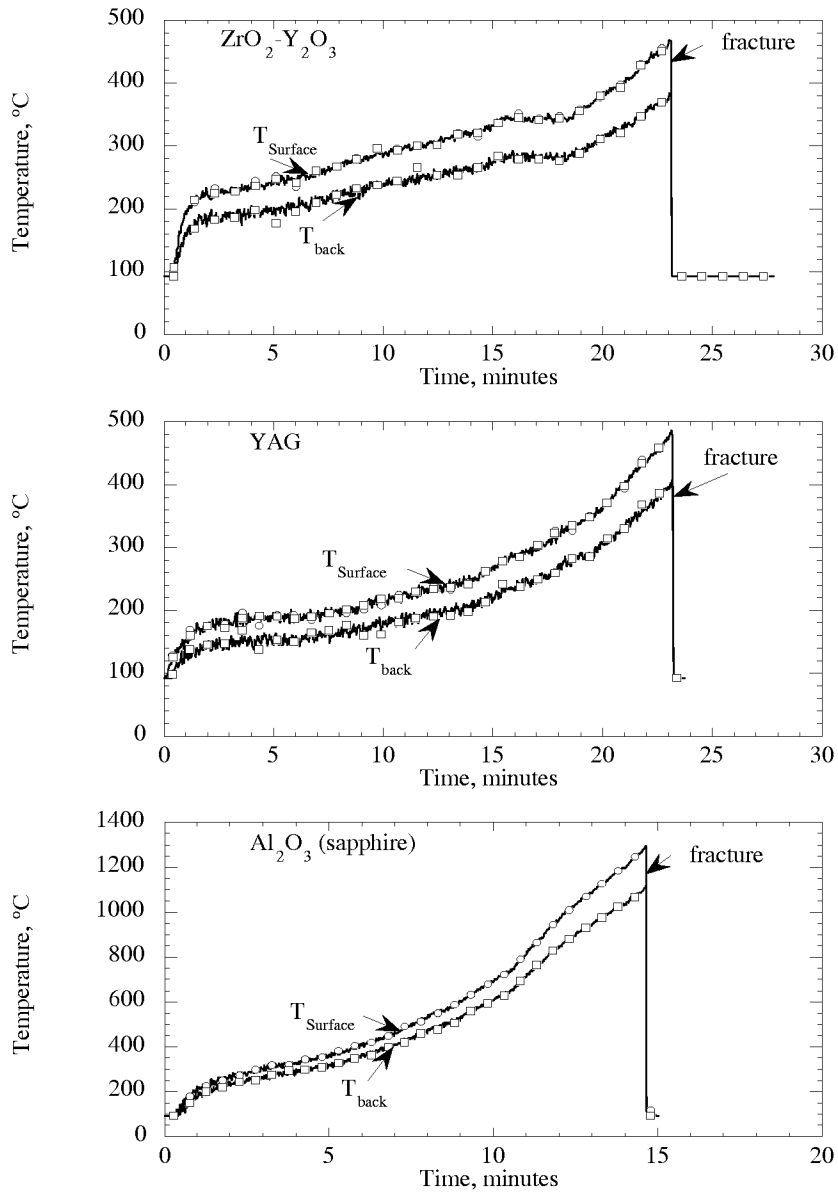
Fig. 5    Examples of the heating profiles of the $Y_2O_3$-doped $ZrO_2$, YAG, and $Al_2O_3$ (sapphire) disk specimens during the laser steady-state thermal gradient testing. The critical temperature difference and corresponding laser power density are thus determined at the onset of cracking.
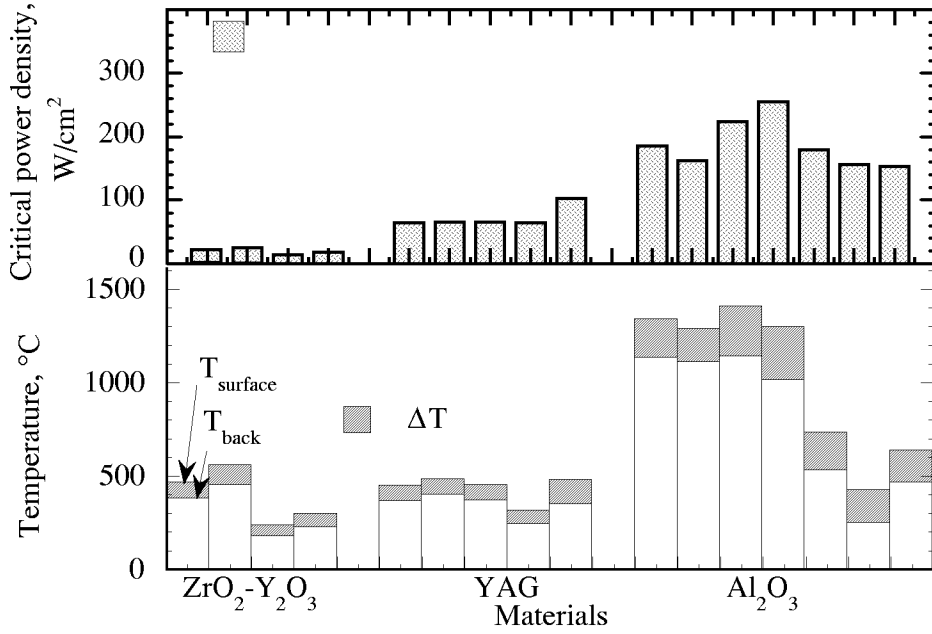
Fig. 6    Critical power densities and critical temperature differences for the $Y_2O_3$-doped $ZrO_2$, YAG, and $Al_2O_3$ (sapphire) disk specimens determined by the laser steady-state thermal gradient testing. The $Al_2O_3$ showed significantly better thermal stress resistance compared to $Y_2O_3$-doped $ZrO_2$ and YAG in terms of the critical temperature difference and power density that cause failure to occur.

(a)                                        (b)
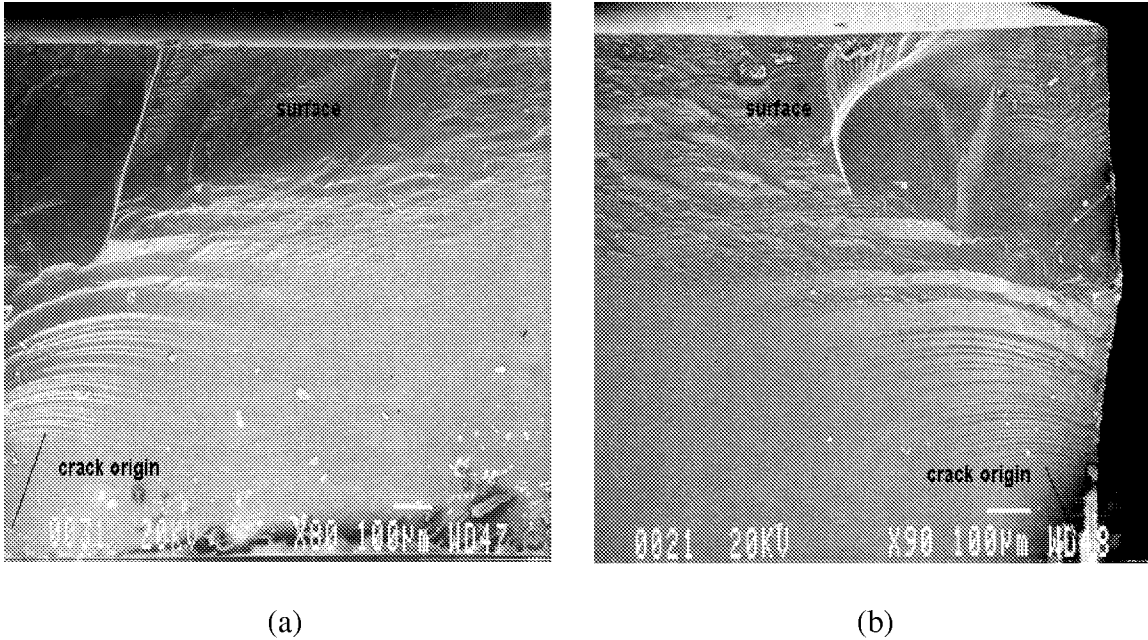
Fig. 7    SEM fractographs of the $Y_2O_3$-doped $ZrO_2$ disk specimens (from two different tests) after the laser steady-state thermal gradient testing. The cracks were initiated near the backside of the specimen surfaces.


Figure 8 shows the temperature profiles of the thermal gradient testing on the single crystal cylindrical specimens under the simulated heating-cooling cycles that may be encountered during the space mission. Maximum temperature differences achieved across the 12.7 mm length were approximately 600°C for $Y_2O_3$-$ZrO_2$ and YAG, and 450°C for MgO and $Al_2O_3$. The temperature gradient was predominantly parallel to the laser heat flux direction, and approximately one-D heating was achieved, as shown in an example of a YAG specimen temperature distribution (Figure 9). The $Y_2O_3$-$ZrO_2$ specimen cracked during the second heating cycle. For the MgO specimen, only a small surface crack was initiated after the first test cycle. For both cases, however, the cracks were initiated at the surface during the heating cycle. The YAG and $Al_2O_3$ specimens did not crack under these test conditions. The cooling cycles seemed to be less damaging for these relatively small size specimens. The $Al_2O_3$ specimen even survived the quench test (at a cooling rate of 658°C/min) due to the laser power loss in this particular test.
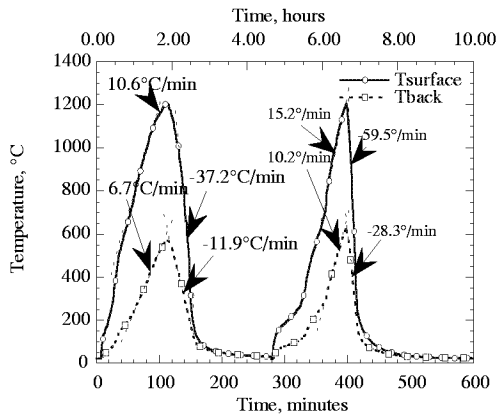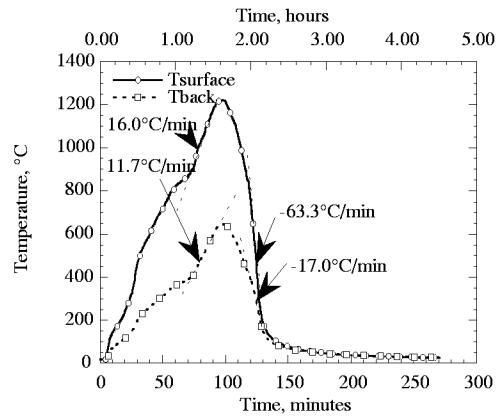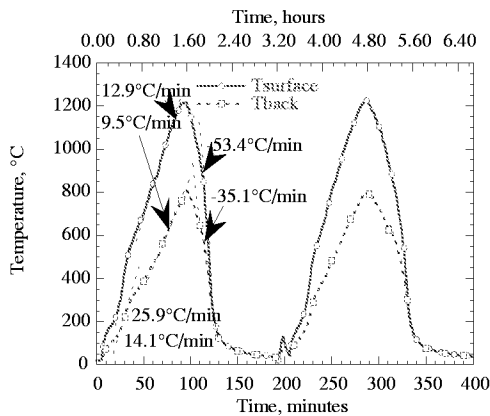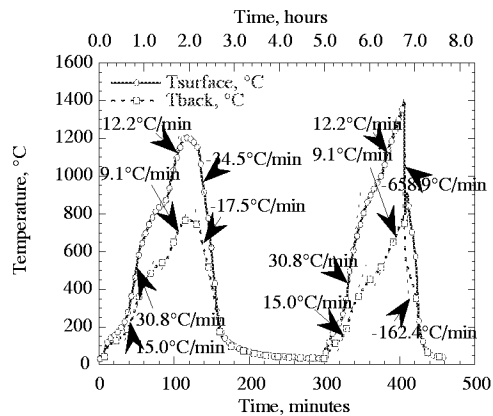
Fig. 8 The thermal gradient testing profiles of the single crystal cylindrical rod specimens to simulate the heating-cooling cycles during the space mission. The maximum heating and cooling rates derived from the temperature-time plots are also labeled in the Figure.
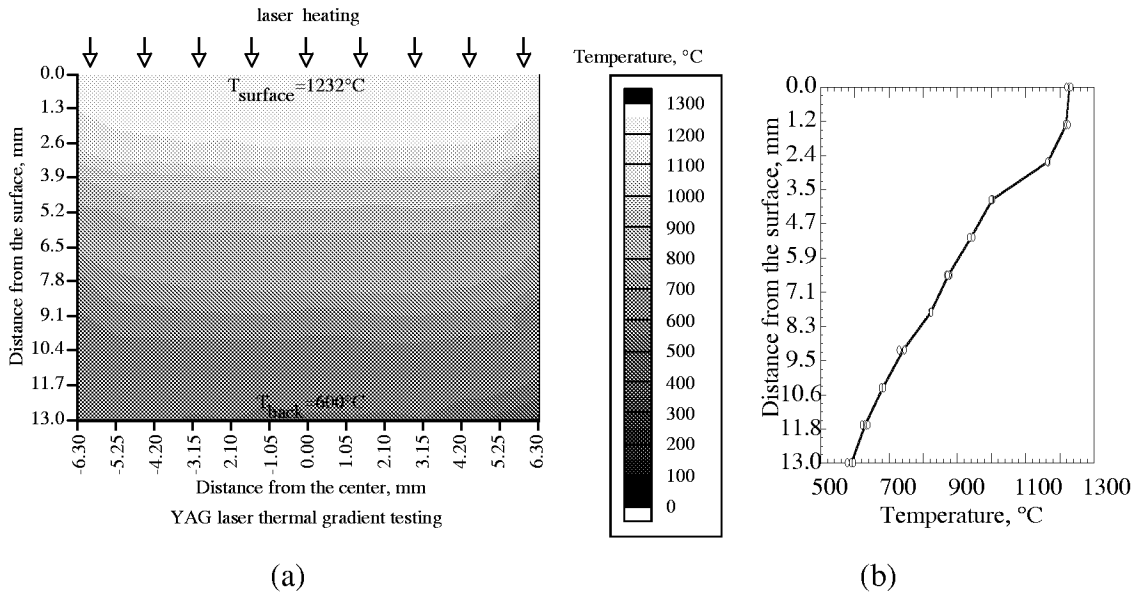
Fig. 9 The thermography temperature distribution in a YAG specimen during the near steady state laser heating (The surface and back side temperatures are approximately 1232°C and 600°C, respectively). (a) Temperature contour distribution in the specimen; (b) temperature distribution along the specimen center region.

For a given material and heating time, the thermal stresses in the specimen increase with the laser power density. Therefore, the critical laser power densities for crystal failure can be determined by laser thermal shock tests under well-controlled transient heating conditions. The results of the laser thermal shock tests showed that the critical power densities at failure were approximately $15.3 \, W/cm^2$, $56.9 \, W/cm^2$, $39.1 \, W/cm^2$ and $109.4 \, W/cm^2$ for $Y_2O_3$-$ZrO_2$, YAG, MgO and $Al_2O_3$ (sapphire) cylindrical specimens, respectively. The $Al_2O_3$ showed the best thermal shock resistance of all the oxide materials tested. The good thermal shock resistance of sapphire is attributed to its high strength, high thermal conductivity and low thermal expansion coefficient.

The failure modes of the single crystal oxides under laser transient thermal shock conditions are relatively complex. From the experiments, it was observed that, for the materials with low thermal conductivity and high thermal expansion, such as $Y_2O_3$-$ZrO_2$

and MgO, the surface cracks could be readily initiated by high compressive stresses and/or the compressive stress-induced (resolved) shear stresses. On the other hand, for the materials with high thermal conductivity and low thermal expansion, such as $Al_2O_3$ and YAG, the cracks are more likely initiated deep in the crystals. Figure 10 illustrates the thermography temperature distributions of YAG and $Al_2O_3$ during the laser heating, and the crystal cracking observed in the middle of the cylindrical specimens. Note that a large crack developed in the $Al_2O_3$ specimen, causing a strong reflection in the thermography image. Therefore, the thermography temperature reading near the crack is no longer valid. Figure 11 illustrates the crack and fracture morphologies of the single crystal oxides after the laser transient thermal shock testing.

For the purpose of demonstration, the stresses in the 12.7 mm long cylindrical specimens have been estimated at the critical laser power densities, based on the temperature distributions measured by thermography and a one-D heat transfer model and under the assumed biaxial stress condition. The material properties used in calculations are listed in Table 1. The results are illustrated in Figure 12. Note that for the much thicker specimen under the transient heating conditions, the stress distributions in the specimen are different from those in the thin specimen case described earlier. In the thick specimen case, after heating up the crystal, a high compressive stress is developed near the surface. The surface compressive stress decreases with the heating time. However, the tensile stress in the inner layer of the crystal increases with time (Figure 12). The peak tensile stress quickly reaches the maximum value and remains almost constant, but it shifts towards the surface for longer time. The backside of the specimen is in compression. It is believed that the surface compressive stress and near-surface tensile stresses are responsible for the observed crystal failures under the laser transient heating conditions.

Table 1. The material properties (average values in the temperature range of 25°C to 1000°C) [7, 10-12] used in thermal stress calculations
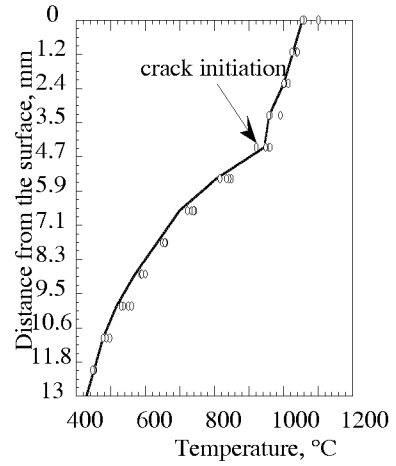
| Materials | Density, g/cm$^3$ | Heat capacity $C_p$, J/g-K | Thermal conductivity , W/cm-K | Thermal expansion coefficient $\alpha$, m/m-K | Young's modulus, E GPa | Poission's ratio, $V$ |
|---|---|---|---|---|---|---|
| ZrO$_2$-Y$_2$O$_3$ | 5.236 | 0.582 | 0.02 | $10.6 \times 10^{-6}$ | 210 | 0.25 |
| YAG | 4.554 | 0.612 | 0.082 | $9.2 \times 10^{-6}$ | 277.5 | 0.25 |
| MgO | 3.585 | 1.005 | 0.052 | $13.7 \times 10^{-6}$ | 245 | 0.3 |
| Al$_2$O$_3$ | 3.38 | 1.15 | 0.12 | $8.6 \times 10^{-6}$ | 380 | 0.22 |
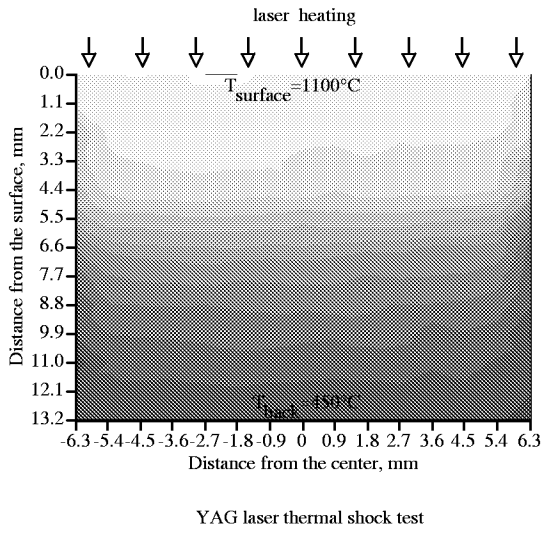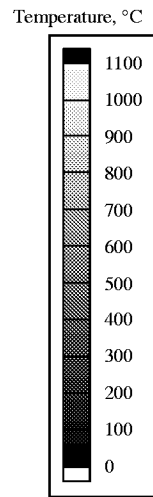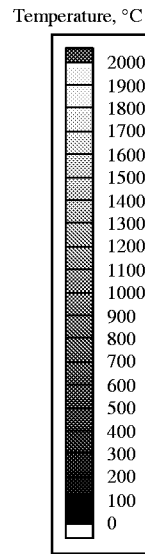
Fig. 10 The temperature distributions in YAG and Al₂O₃ specimens during the laser thermal shock testing after 50 sec heating at the critical laser powers. (a and b) Temperature contour and line distributions in YAG; (c and d) temperature contour and line distributions in Al₂O₃.
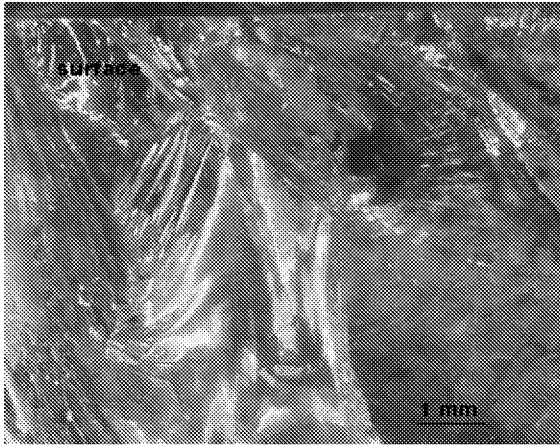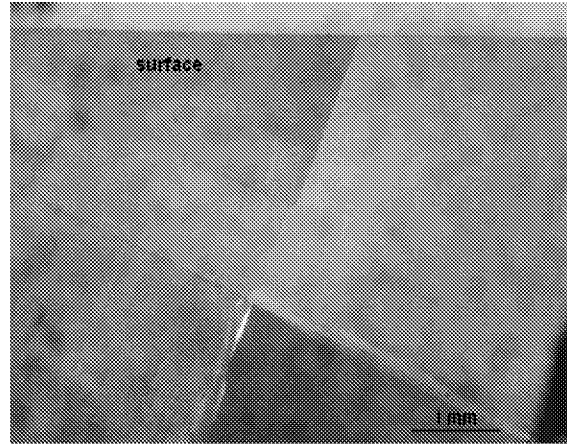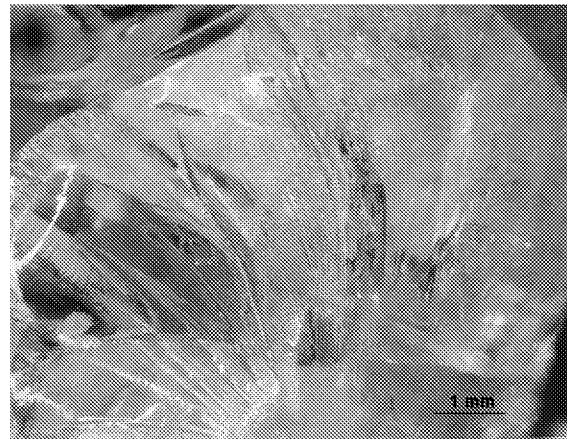
(a)  (b)
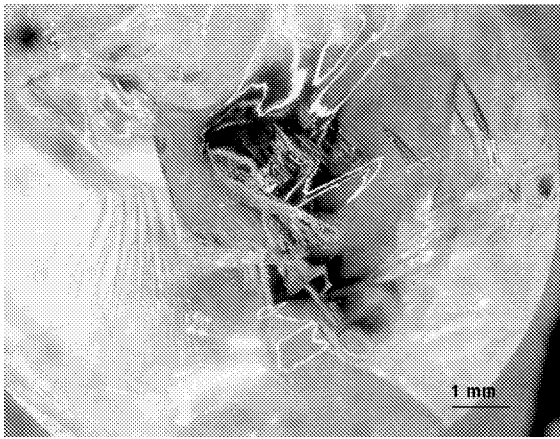
(c)  (d)

Fig. 11  The crack and fracture morphologies (optical microscopy) of the single crystal oxides after the laser thermal transient testing. (a) Surface initiated cracks and the subsequent crack propagation in $ZrO_2$-$Y_2O_3$; (b) surface shear stress initiated cleavage along the (110) plane in MgO; (c) the cracked surface in the middle of the YAG specimen;  (d) the cracked surface in the middle of the $Al_2O_3$ specimen.
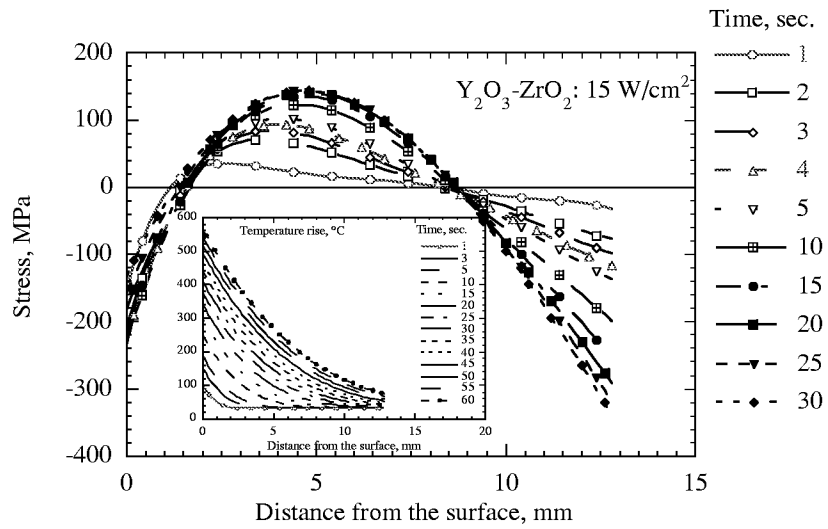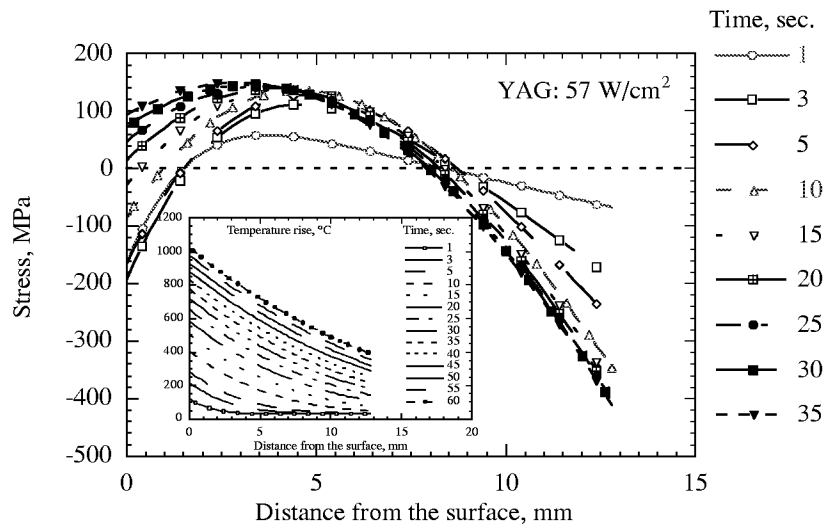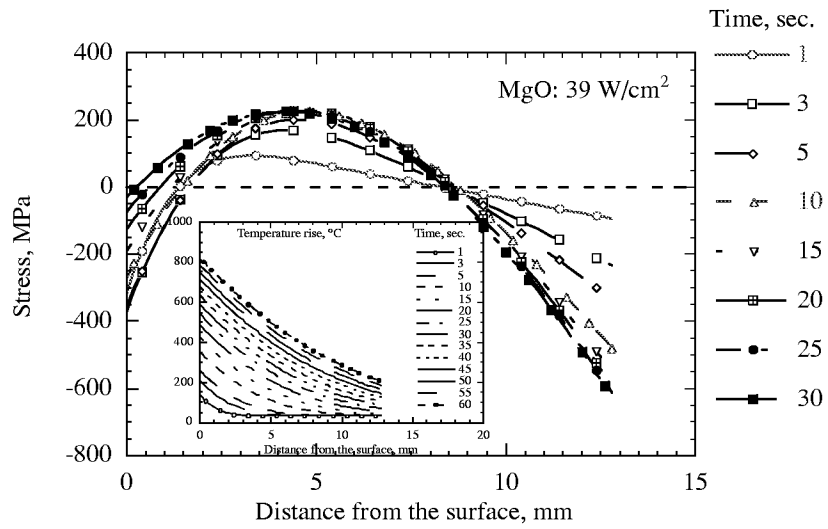
Fig. 12 The modeled thermal stress distributions in the 12.7 mm long cylindrical specimens during laser transient thermal shock testing at the critical laser power densities.

(c) MgO



(d) Al₂O₃

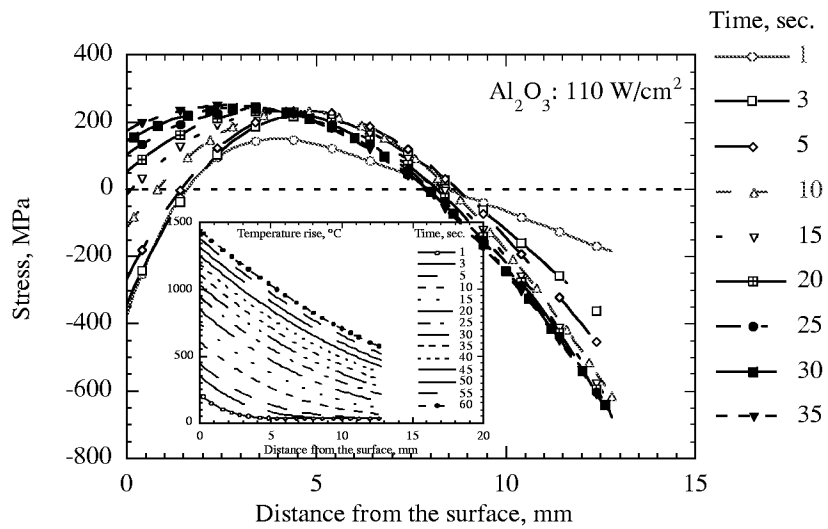Fig. 12   (Continued) The modeled thermal stress distributions in the 12.7 mm long cylindrical specimens during laser transient thermal shock testing at the critical laser power densities.

# CONCLUDING REMARKS

A laser thermal shock test approach has been proposed for evaluating thermo-mechanical stability of single crystal oxide refractive concentrator materials under simulated mission conditions. This technique is especially useful in determining the thermal stress resistance of single crystal oxides under steady state and transient thermal heating, thus providing vital information for the component design and material development.

Thermal shock resistance of several candidate single crystal oxide concentrator materials, namely yttria-stabilized zirconia, yttrium aluminum garnet and magnesium oxide and sapphire was investigated. The experiments showed that the single crystal sapphire can sustain the highest temperature gradient and heating-cooling rate, as compared to the other oxides, thus exhibiting the best thermal shock resistance.

# ACKNOWLEDGMENTS

# REFERENCES

[1]    J. A. Soules, D. R. Buchele, C. H. Castle, and R. P. Macosko, "Design and Fabrication of a Dielectric Total Internal Reflecting Solar Concentrator and Associated Flux Extractor for Extreme High Temperature (2500K) Applications," NASA Lewis Research Center, Cleveland, NASA CR 204145, November 1997.

[2]     X. Ning, R. Winston, and J. O'Gallagher, "Dielectric Totally Internally Reflecting Concentrators," *Applied Optics*, vol. 26, pp. 300-305, 1987.

[3]     S. M. Geng, "Transient Thermal Heat-up of a Refractive Secondary Solar Concentrator," *To be published*, 1998.

[4]     J. T. Luxon and D. E. Parker, *Industrial Lasers and Their Applications*. Englewood Cliffs, New Jersey: Prentice-Hall, Inc., 1985.

[5]     D. Zhu and R. A. Miller, "Thermal Fatigue Testing of $ZrO_2$-$Y_2O_3$ Thermal Barrier Coating Systems using A High Power Laser," NASA Lewis Research Center, Cleveland, Technical Memorandum 107439, June 1997.

[6]     D. Zhu and R. A. Miller, "Investigation of Thermal High Cycle and Low Cycle Fatigue Mechanisms of Thick Thermal Barrier Coatings," *Materials Science and Engineering*, vol. A245, pp. 212-223, 1998.

[7]     W. D. Kingery, "Factors Affecting Thermal Stress Resistance of Ceramic Materials," *Journal of the American Ceramic Society*, vol. 38, pp. 3-15, 1955.

[8]     D. P. Hasselman, "Thermal Stress Resistance of Engineering Ceramics," *Materials Science and Engineering*, vol. 71, pp. 251-264, 1985.

[9]     W. B. Hillig, "A Methodology for Estimating the Mechanical Properties of Oxides at High Temperature," *Journal of the American Ceramic Society*, vol. 76, pp. 129-138, 1993.

[10]    "$Nd^{3+}$: $Y_3Al_5O_{12}$ (YAG) Physical Properties," *personal communication*, 1997.

[11]    W. P. Holbrook, J. B. Wachtman, C. Schnitzer, and L. M. Sheppard, "Ceramic Source," vol. 8, 1992-1993.

[12]    D. Zhu and R. A. Miller, "Investigation of Thermal Fatigue Behavior of Thermal Barrier Coating Systems," *Surface and Coatings Technology*, vol. 94-95, pp. 94-101, 1997.

# REPORT DOCUMENTATION PAGE

Form Approved
OMB No. 0704-0188

| 1. AGENCY USE ONLY (Leave blank) | 2. REPORT DATE | 3. REPORT TYPE AND DATES COVERED |
|---|---|---|
| | February 1999 | Technical Memorandum |

**4. TITLE AND SUBTITLE**

Thermal-Mechanical Stability of Single Crystal Oxide Refractive Concentrators for High-Temperature Solar Thermal Propulsion

**5. FUNDING NUMBERS**

WU–953–73–10–00

**6. AUTHOR(S)**

Dongming Zhu, Nathan S. Jacobson, and Robert A. Miller

**7. PERFORMING ORGANIZATION NAME(S) AND ADDRESS(ES)**

National Aeronautics and Space Administration
Lewis Research Center
Cleveland, Ohio 44135–3191

**8. PERFORMING ORGANIZATION REPORT NUMBER**

E–11524

**9. SPONSORING/MONITORING AGENCY NAME(S) AND ADDRESS(ES)**

National Aeronautics and Space Administration
Washington, DC 20546–0001

**10. SPONSORING/MONITORING AGENCY REPORT NUMBER**

NASA TM—1999-208899

**11. SUPPLEMENTARY NOTES**

Prepared for the 1999 International Solar Energy Conference, Renewable and Advanced Energy Systems for the 21st Century sponsored by the American Society of Mechanical Engineers, Lahaina, Maui, Hawaii, April 11–15, 1999. Responsible person, Dongming Zhu, organization code 5160, (216) 433–5422.

**12a. DISTRIBUTION/AVAILABILITY STATEMENT**

Unclassified - Unlimited
Subject Categories: 23 and 20          Distribution: Nonstandard

This publication is available from the NASA Center for AeroSpace Information, (301) 621–0390.

**12b. DISTRIBUTION CODE**

**13. ABSTRACT (Maximum 200 words)**

Single crystal oxides such as yttria-stabilized zirconia ($Y_2O_3$-$ZrO_2$), yttrium aluminum garnet ($Y_3Al_5O_{12}$, or YAG), magnesium oxide (MgO) and sapphire ($Al_2O_3$) are candidate refractive secondary concentrator materials for high temperature solar propulsion applications. However, thermo-mechanical reliability of these components in severe thermal environments during the space mission sun/shade transition is of great concern. Simulated mission tests are important for evaluating these candidate oxide materials under a variety of transient and steady-state heat flux conditions, and thus provide vital information for the component design. In this paper, a controlled heat flux thermal shock test approach is established for the single crystal oxide materials using a 3.0 kW continuous wave $CO_2$ laser, with a wavelength 10.6 micron. Thermal fracture behavior and failure mechanisms of these oxide materials are investigated and critical temperature gradients are determined under various temperature and heating conditions. The test results show that single crystal sapphire is able to sustain the highest temperature gradient and heating-cooling rate, and thus exhibit the best thermal shock resistance, as compared to the yttria-stabilized zirconia, yttrium aluminum garnet and magnesium oxide.

**14. SUBJECT TERMS**

Single crystal oxides; Solar concentrators; High temperature thermal gradient testing

**15. NUMBER OF PAGES**
28

**16. PRICE CODE**
A03

| 17. SECURITY CLASSIFICATION OF REPORT | 18. SECURITY CLASSIFICATION OF THIS PAGE | 19. SECURITY CLASSIFICATION OF ABSTRACT | 20. LIMITATION OF ABSTRACT |
|---|---|---|---|
| Unclassified | Unclassified | Unclassified | |

NSN 7540-01-280-5500

Standard Form 298 (Rev. 2-89)
Prescribed by ANSI Std. Z39-18
298-102